Faraday Discussions

Cite this: *Faraday Discuss.*, 2025, **259**, 45

PAPER

View Article Online
View Journal | View Issue

Immune cell activation produces locally scrambled foci of plasma membrane lipids

Daryna Sputay,[a] Milka Doktorova,[b] Sze Ham Chan,[a] Emma Han Guo,[a] Hong-Yin Wang,[a] Joseph H. Lorent,[c] Ilya Levental *[a] and Kandice R. Levental *[a]

Received 20th December 2024, Accepted 11th February 2025
DOI: 10.1039/d4fd00205a

Most eukaryotic cells maintain a large disparity in lipid compositions between the cytosolic and external leaflets of the plasma membrane (PM) bilayer. This lipid asymmetry is maintained by energy-consuming flippase enzymes that selectively drive phospholipids into the cytosolic leaflet, often against large concentration gradients. Scramblases, activated by intracellular Ca^{2+} or apoptotic signaling, shuttle phospholipids down their concentration gradient to release lipid asymmetry. Such scrambling is typically evidenced by exposure of phosphatidylserine (PS) to the external leaflet and is associated with many physiological processes, most notably blood clotting and cell death, but also activation of immune cells. Here, we show that both PS and phosphatidylethanolamine (PE) appear on the PM external leaflet following immune receptor-mediated activation of mast cells. We also observe similar effects in T cells. Importantly, in contrast to wholesale release of PM asymmetry induced by calcium ionophores or apoptosis, we show that scrambling in activated immune cells is focal, with small, stable regions of surface exposed PS. These scrambled foci are calcium dependent, have lower lipid packing than their surrounding outer leaflet, and are reversible. These observations of local, transient scrambling during physiological activation of healthy immune cells suggest important roles for the lateral and transbilayer organization of membrane lipids.

Introduction

Membranes are involved in nearly all aspects of cellular physiology, with their functions determined by the composition and organization of their constituent lipids and proteins. A ubiquitous feature of eukaryote plasma membranes (PM) is a highly disparate distribution of lipids between the two leaflets of the bilayer, termed lipid asymmetry.[1] The outer (exoplasmic) leaflet is generally enriched in

[a]*Department of Molecular Physiology and Biological Physics, University of Virginia, USA. E-mail: il2sy@virginia.edu; krl6c@virginia.edu*
[b]*Department of Biochemistry and Biophysics, Stockholm University, Science for Life Laboratory, Sweden*
[c]*Cellular and Molecular Pharmacology (FACM), Louvain Drug Research Institute, UCLouvain, Belgium*

choline-headgroup lipids with relatively saturated acyl chains.[1,2] The inner (cytoplasmic) leaflet of PM is composed of lipids with negatively charged headgroups (phosphatidylserine (PS) and phosphatidic acid (PA)), amine headgroup phosphatidylethanolamine (PE), and phosphoinositides (PI and PIPs). The high concentration of anionic phospholipids (PLs) in the PM inner leaflet contributes to recruitment of membrane-proximal signaling proteins, which can interact with the cytoplasmic leaflet *via* electrostatic interactions with polybasic protein domains.[3–5] These electrostatic protein–lipid interactions can regulate signaling pathways that control cell physiology.[4] Further, it was recently shown that the distinct compositions of the two bilayer leaflets produce distinct biophysical properties, with unsaturated-lipid-rich inner leaflets being less tightly packed and more fluid (*i.e.* diffusive) than the more saturated outer leaflets.[2,6] Lipid asymmetry also produces other biophysical effects: *e.g.* asymmetric membranes can be stiffer than counterparts with identical lipid compositions but symmetric distributions.[7] This effect has been attributed to leaflet stresses resulting from imbalanced total abundance of phospholipids between leaflets,[8,9] termed differential stress.

Building and maintaining lipid asymmetry is energetically expensive, requiring ATP-dependent transport of billions of phospholipids against sharp concentration gradients.[10] Specific transmembrane protein transporters termed flippases (often P4-ATPases) sustain the transbilayer gradient of phospholipids, constitutively translocating them against a concentration gradient.[11] Lipid channels called scramblases rapidly redistribute phospholipids down their concentration gradient in an ATP-independent and apparently weakly selective manner to release membrane asymmetry.[12] This process can be reported by visualization of the externalized PS on the exoplasmic leaflet using extracellular fluorescent PS-binding probes like AnnexinV (AnxV) or LactadherinC2 (LactC2).[13,14] In apoptosis, the caspase-activated scramblase Xk-related protein 8 (XKR8) is activated to shuttle PS across the whole PM, apparently fully destroying PM asymmetry.[15–17] Several family members of the transmembrane protein 16 (TMEM16) family (most notably TMEM16F) are Ca^{2+}-activated lipid channels, which also translocate PS to the outer leaflet in various cellular contexts.[18–20] While these proteins have been extensively implicated in cellular function and disease, the physiological roles of steady-state membrane asymmetry and its regulated release remain poorly understood. In this context, it has been shown that lipid scrambling affects the biophysical properties of membrane leaflets.[21] PM outer leaflets become less tightly packed, consistent with their gaining lipids with unsaturated acyl chains from the inner leaflet. Further, the overall properties (*e.g.* lipid packing, permeability, and/or stiffness) of the scrambled PM bilayer appear to be distinct from a steady-state asymmetric one.[21]

Historically, most research into lipid asymmetry focused on apoptosis and other forms of cell death, where its release exposes PS on the outer leaflet, marking dead cells for clearance by macrophages.[18,22,23] More recently, it has become clear that lipid scrambling also occurs during physiological processes in healthy cells. Regulated PM scrambling has been reported in cell–cell fusion,[24–28] release of extracellular vesicles,[29,30] blood clotting[20,23] and immune cells signaling.[31–34] These effects can have critical consequences, as scramblase deficiency leads to Scott syndrome, a blood coagulation disorder characterized by impaired membrane scrambling during platelet activation. Scrambling is also important for repairing plasma membrane damage by bacterial pore-forming

agents: TMEM16F-mediated lipid scrambling increases PM membrane fluidity after damage and promotes membrane blebbing and shedding of extracellular vesicles containing damaged lipids, supporting PM repair and cell survival.[35] Finally, exposure of PE has been implicated in cell division, regulating the final steps of cytokinesis.[36]

Lipid scrambling (evidenced by PS exposure) upon activation of signaling through stimulation of cell surface immune receptors has been reported in multiple immune cell types, including T cells,[31] B cells,[32] neutrophils,[33] monocytes,[37] natural killer cells,[38] and mast cells.[34] The specific functions and mechanisms by which this lipid redistribution is implicated in functional immune signaling remain poorly understood. In T cells, scrambling through TMEM16F may reduce the electrostatic potential of the inner PM leaflet, potentially enhancing T cell receptor (TCR) phosphorylation[39] *via* electrostatic protein–membrane interactions. In support of this hypothesis, reducing expression of TMEM16F eliminates PM scrambling and decreases TCR phosphorylation, halting signal amplification.[39] In notable contrast, others have shown that TMEM16F terminates, rather than amplifies TCR signaling, to avoid T cell exhaustion.[40] Thus, while TMEM16F-mediated PM scrambling has important effects on immune cell signaling, the precise effects remain unresolved.

Here, we use fluorescence microscopy to characterize membrane changes during receptor-mediated activation of mast and T cells. We find that activated immune cells exhibit a distinct mode of PM scrambling from apoptotic scrambling, characterized by distinct foci of externalized PS and PE that persist for 1–2 h before resolving back into an asymmetric state. These foci are dependent on extracellular calcium and exhibit decreased lipid packing compared to their surrounding PM. These observations reveal that immune cell activation induces localized and transient lipid scrambling that locally change the biophysical properties of the PM outer leaflet. These effects are notably distinct from wholesale PM scrambling, prompting hypotheses about the physiological functions of lipid asymmetry and its regulated release.

Results

There have been extensive observations of PS scrambling induced by apoptosis or calcium ionophores.[16,18,20] We reproduced these findings in rat basophilic leukemia (RBL) cells, by imaging recombinant PS probes binding to the external leaflet of the PM after staurosporine treatment to induce apoptosis or ionophore to increase cytosolic [Ca^{2+}]. Staurosporine treatment for 4 h induced major changes to cell morphology, including membrane blebbing, consistent with apoptosis. As expected, these cells stained brightly with AnxV, a calcium-dependent PS-binding protein (Fig. 1A, top) and with recombinant LactC2, a calcium-independent and monomeric probe for surface-exposed PS (Fig. 1B, left). Treating RBL cells with the ionophore A23187 to increase cytosolic calcium also produced extensive PS exposure across the entire cell surface (Fig. 1A and B).

Antigen-induced activation of mast cells produces focal PM scrambling

RBL cells are a popular model for mast cell signaling because their signaling can be activated by physiologically relevant stimuli. Namely, these cells bind IgE

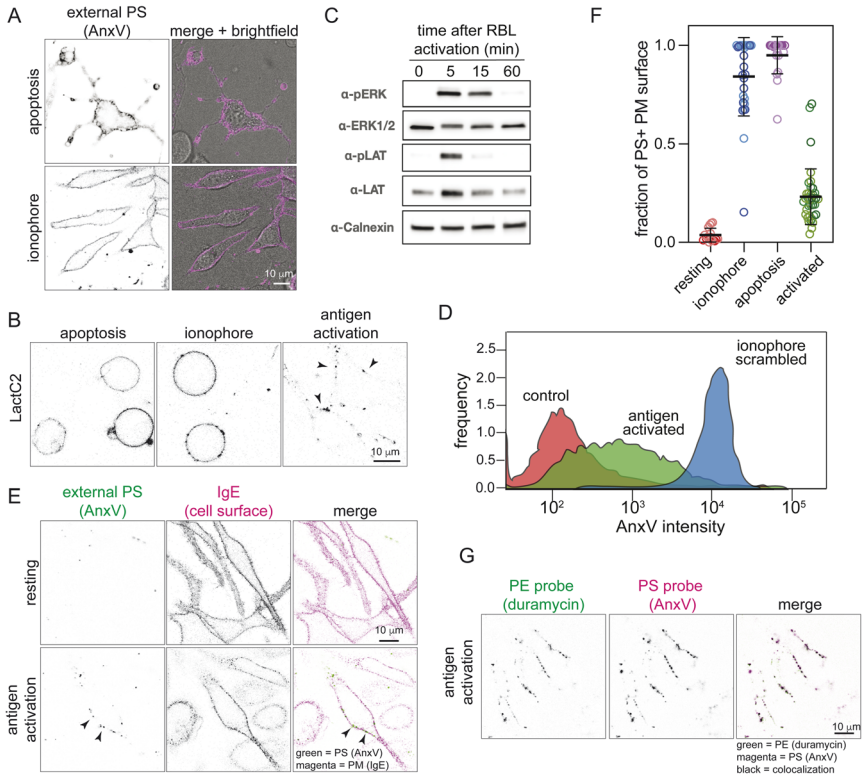

Fig. 1 Antigen-mediated activation of mast cells induces focal scrambling. (A) Top: apoptosis induction in RBL-2H3 cells by staurosporine leads to wholesale loss of PM asymmetry, reported by staining with AnnexinV-AF647 (AnxV). Bottom: similar whole-cell scrambling is induced by treatment with the calcium ionophore A23187. Left panel shows the fluorescent signal intensity inverted (see note below at end of this figure legend), and right panel is an image with the brightfield (gray scale) and fluorescence (magenta pseudocolor) merged. (B) Similar effects are observed by staining with the monomeric PS probe LactC2. Antigen activation results in focal exposure of PS as observed by LactC2 punctae (arrowheads, right). (C) RBL activation induced by treating anti-DNP IgE primed cells with the crosslinking antigen DNP-BSA. Western blotting reveals the phosphorylation of ERK and LAT expected of antigen-mediated activation. (D) Flow cytometry comparison of AnxV staining intensity between non-activated, activated (for 30 min), and ionophore scrambled (after 5 min) RBL cells. (E) RBL cells primed with anti-DNP IgE (IgE-AF555) show focal scrambling. Activation (by DNP-BSA) produced foci of AnxV binding on the PM (arrow heads), indicative of exposed PS. IgE-555 shown as a fiducial marker to visualize the PM. In the inverted merged images, PM (marked by IgE-555) is magenta, and AnxV is green. (F) Quantification of the fraction of the RBL PM surface positive for PS-probe LactC2. Dots represent individual cells with cells from independent repeats shown in different shades ($N \geq 2$). (G) Simultaneous staining for PE (duramycin-PEG-GFP, left) and PS (AnxV-647, middle) on RBL cells following antigen activation shows colocalization (black, right) of the two probes on the outer PM leaflet. Note: in all fluorescence images in this figure, the inverse of the signal is shown for better contrast on screens and paper. Darker pixels represent higher fluorescent signal. In E and G, merged pseudocolored images are shown on the right.

antibodies *via* the antibody receptor FcεRI on their PMs. Addition of specific multivalent antigens crosslinks the receptor, inducing a cascade of signals that ultimately lead to calcium mobilization, degranulation, and cytokine secretion.[41] Here, we used a classical approach to activate RBL cells by priming with IgE against the hapten dinitrophenol (DNP) and then treating with the multivalent antigen DNP-BSA. This treatment induced phosphorylation of Linker for Activation of T-cells (LAT) and extracellular signal-regulated kinase (ERK), as expected of mast cell activation (Fig. 1C). As increased cytosolic calcium is a central feature of immune cell activation,[42] we hypothesized that it may also activate lipid scrambling, similar to calcium ionophore treatment. Indeed, flow cytometry revealed that RBL activation leads to increased staining with externally applied AnxV (Fig. 1D), similar to previous reports;[34] however, AnxV staining of activated RBLs was substantially lower (more than an order of magnitude) than ionophore-induced scrambling, suggesting a distinct form of scrambling. Using confocal microscopy to visualize externalized PS (*via* AnxV) on activated RBLs, we found PS staining in bright, stable foci (Fig. 1E, bottom). Similar foci were also observed with LactC2 (Fig. 1B, right). The contrast between activation- and apoptosis/ionomycin-induced scrambling can be quantified *via* the fraction of the PM surface labeled with the PS-binding probe (Fig. 1F, LactC2 was used for this quantification because it is monomeric). Resting cells had essentially undetectable LactC2 binding (consistent with minimal PS exposure), while apoptotic and ionophore-treated cells had PS exposed over the entire PM outer leaflet. In contrast, activated RBL cells showed external PS labeling over ~20% of the PM surface (Fig. 1F). The PS-positive foci also contained externalized phosphatidylethanolamine (PE), as revealed by co-labeling of AnxV-positive foci with the PE-binding probe duramycin (Fig. 1G).

Since other immune cells use similar calcium-mediated signaling during their activation, we hypothesized that they may also locally scramble their PMs. To test this prediction, we used a well-established method of activating Jurkat T-cells by plating them onto coverslips coated with an anti-CD3 (TCR) antibody (OKT3);[43] activation was evidenced by phosphorylation of LAT and ERK (Fig. 2A), as in mast cells (Fig. 1C). As in activated RBL cells, total internal reflection fluorescence (TIRF) microscopy showed bright foci of AnxV staining on the basal (*i.e.* OKT3-contacting) surface of activated Jurkat cells, revealing local sites of PS scrambling (Fig. 2B). Interestingly, a more coverslip-distal plane imaged by epifluorescence had minimal AnxV staining (Fig. 2B, right), suggesting that scrambling only occurred on the cell surface that was transducing the activating signal.

These findings reveal that immune-receptor mediated activation of mast and T cells causes focal release of PM asymmetry evidenced by scrambling of major inner leaflet phospholipids.

Scrambled foci have reduced lipid packing

It was previously shown that outer leaflets of scrambled PMs have lower lipid packing than outer leaflets of asymmetric PMs of cells at steady-state;[2] similar effects were reported in apoptotic cells.[44,45] Thus, we hypothesized that the PS-positive foci produced during immune cell activation would also have lower lipid packing. We measured lipid packing in the exoplasmic PM leaflet by imaging fluorescence emission lifetime of the polarity-sensitive probe Di-4-ANEPPDHQ

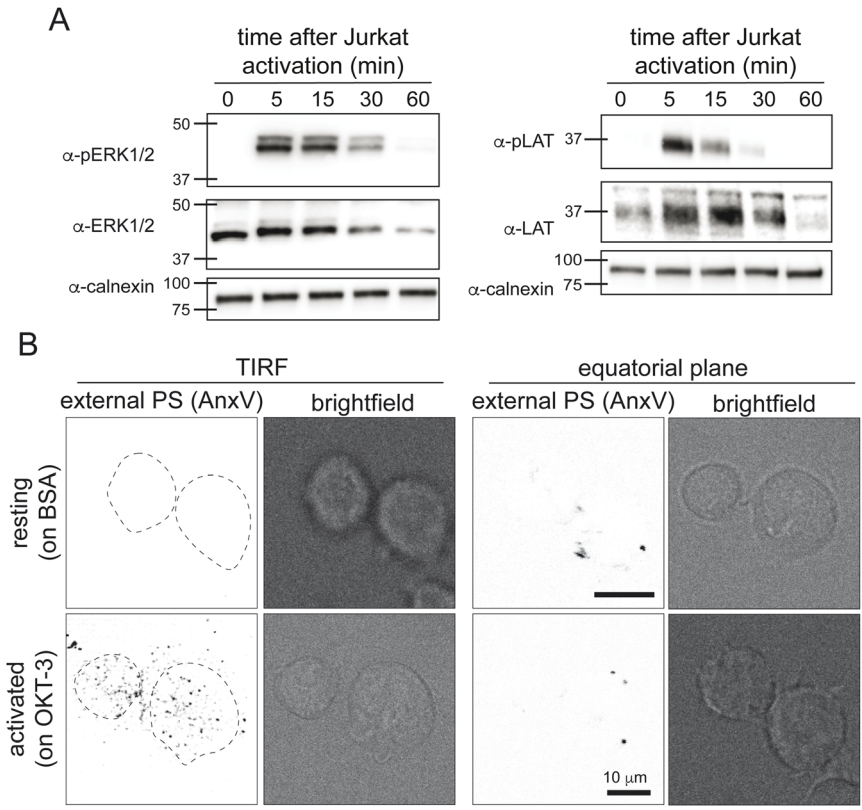

Fig. 2 Activation of T cells induces focal scrambling. (A) Jurkat activation induced by treating cells with anti-CD3. Western blotting reveals the phosphorylation of ERK and LAT expected of antigen-mediated activation. (B) Jurkat T cells exhibit focal PM scrambling when activated by an anti-CD3 (*i.e.* OKT3) coated glass surface. Foci are visible on the basal PM imaged in TIRF, whereas no PS exposure is observed on the cell PM mid-plane. All fluorescence images in this figure are inverted, with darker pixels representing more fluorescent signal.

(Di4), a widely used proxy for lipid packing.[2,21,46,47] Wholesale PM scrambling by ionomycin or apoptosis reduced outer leaflet lipid packing, evidenced by greatly reduced Di4 lifetimes (Fig. 3A and B). This effect is consistent with the introduction of unsaturated lipids from the inner leaflet. Di4 lifetime was also notably reduced in activated RBL cells, but the magnitude of the reduction was much smaller than for ionophore or apoptosis treatments (Fig. 3A). This effect was due to foci of reduced Di4 lifetime, with the remainder of the PM remaining similar to resting cells (Fig. 3B). This effect could be quantified by measuring Di4 lifetime along the cell periphery: in both resting and ionophore-treated cells, lifetime was generally homogeneous whereas the PM of activated cells alternated between a 'resting-like' bulk and 'scrambled-like' foci (Fig. 3C). This lateral heterogeneity, summarized as the range in measured lifetime values, was significantly greater in activated cells than either resting or fully scrambled (Fig. 3D). We confirmed that these foci of lower lipid packing were sites of PS scrambling by their co-staining

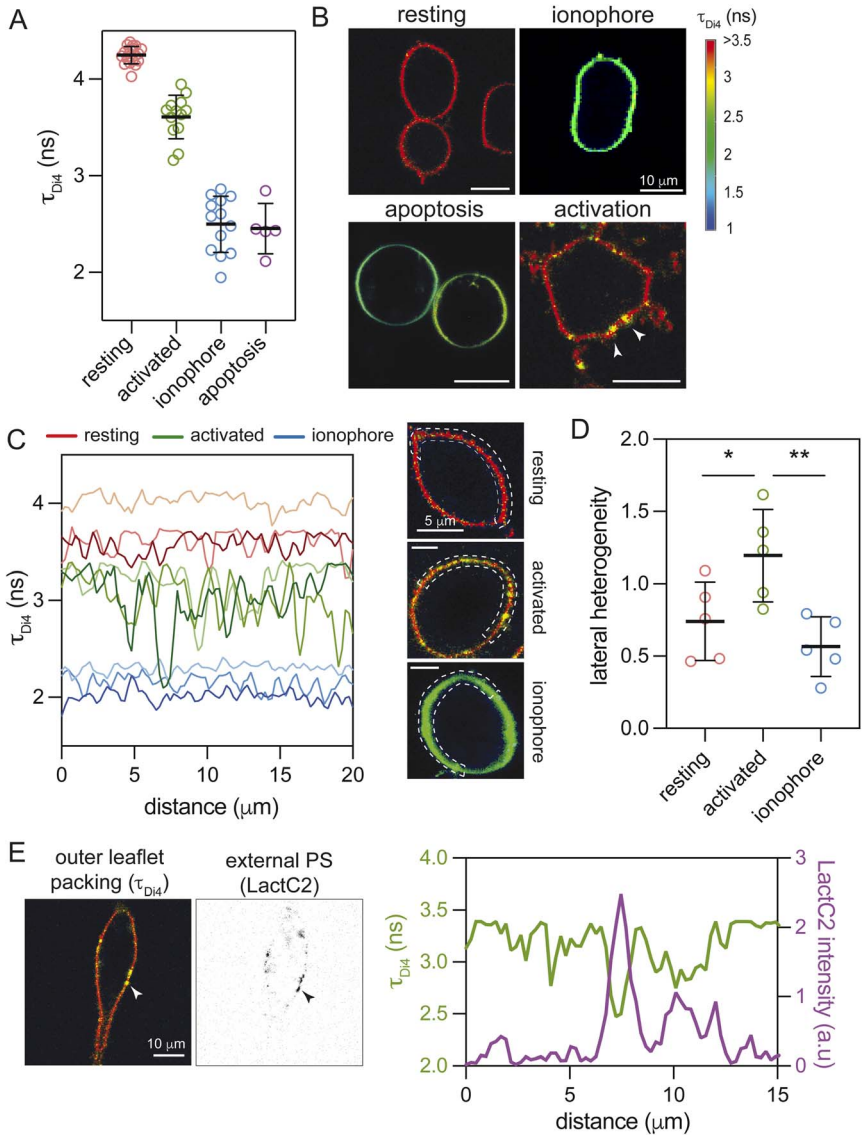

Fig. 3 Scrambled foci have reduced lipid packing. (A) Measurement of PM outer leaflet packing *via* Di4 fluorescence lifetime imaging (FLIM) in mast cells. Scrambling by apoptosis or ionophore dramatically reduces outer leaflet packing, while activation has a smaller but nevertheless prominent effect. Dots represent mean lifetime values from individual cells. (B) Representative Di4 fluorescence lifetime imaging microscopy (FLIM) images show that activated RBL cells have foci of reduced lipid packing (arrows). Ionophore and apoptotic cell PMs have a uniformly lower lifetime (*e.g.* are less packed). (C) Di4 lifetime profiles of resting (shades of red), activated (green), and ionophore-scrambled cells (blue) illustrate PM packing changes along the surface, with activated mast cells exhibiting regions of lower lipid packing within a bulk PM whose packing is similar to resting cells. Representative PM line traces are taken from the boxed region of the confocal FLIM images shown on right. (D) The lateral heterogeneity in lipid packing is greater in activated mast cells than either resting or fully scrambled. (E) Foci of lower lipid packing revealed by Di4 lifetime are colocalized with foci of externalized PS (LactC2 staining, black). Di4 lifetime and LactC2 intensity along the membrane surface in the region indicated by the arrow are shown on the right.

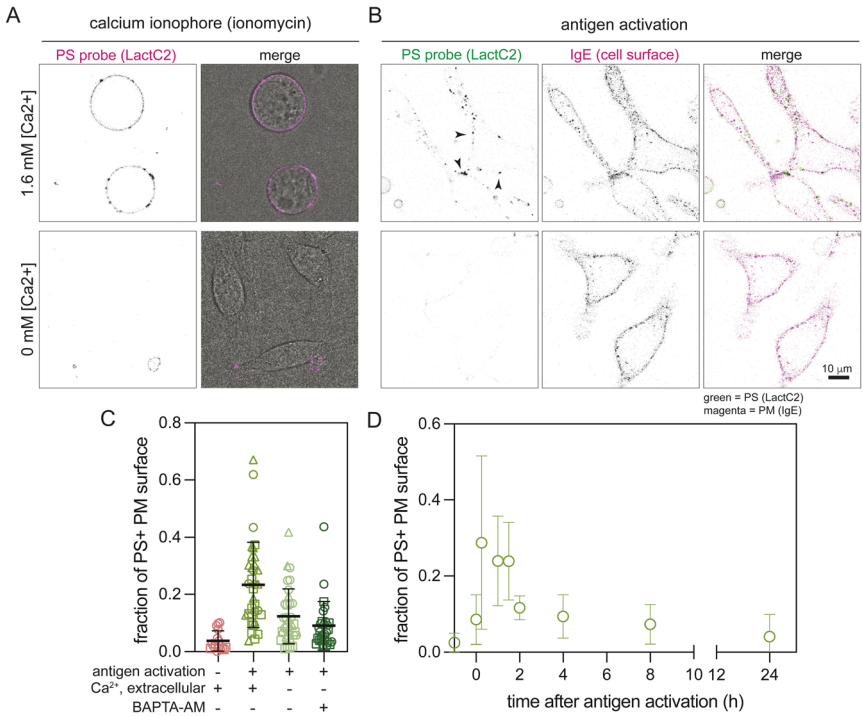

Fig. 4 Calcium dependence and kinetics of scrambling in activated mast cells. (A and B) PS externalization due to ionophore treatment (ionomycin, (A)) or antigen activation (B) in RBL-2H3 cells is dependent on external calcium, as visualized by LactC2 binding. Cells treated in calcium-free buffer had minimal PS externalization in both conditions. (A) Left column shows LactC2-mCherry binding, right shows a merge with LactC2 fluorescence and brightfield. (B) Left column shows LactC2-mClover binding, middle column shows IgE-555 as a fiducial marker to visualize the PM, right, shows merged LactC2 (green) and IgE (magenta); colocalization of external PS (LactC2) and the PM marker (IgE-555) are shown as black. (C) Quantification of PM surface fraction positive for staining by the PS-probe LactC2. Absence of extracellular calcium reduced scrambling by ~50% and further chelation of intracellular calcium (by BAPTA-AM) had only a minimal additional effect. Dots represent individual cells with different shapes representing cells from independent repeats ($N \geq 2$). (D) Temporal profile of the PS-probe positive PM surface fraction after antigen-mediated RBL activation. PS externalization peaked by ~15 min after antigen addition and remained stable for ~1.5 h, before gradually returning to completely asymmetric by ~4 h.

with the PS marker LactC2 (Fig. 3E). Thus, immune cell activation produced focal PM regions with externalized inner leaflet lipids and reduced lipid packing.

Activation-induced scrambling requires external calcium and is reversible

We hypothesized that scrambled foci produced during immune cell activation result from the transient increases in cytosolic calcium that are a hallmark of immune signaling.[48] Calcium fluxes during signaling may be sufficient to activate the non-apoptotic scramblase TMEM16F, which is gated by cytosolic calcium.[18,20] To evaluate this possibility, we treated cells without external calcium and imaged scrambling by external LactC2. As expected, the absence of external calcium

completely blocked scrambling by the ionophore A23187 (Fig. 4A). Similarly, absence of external calcium significantly reduced the frequency of LactC2-positive foci in activated RBLs (Fig. 4B). Quantification of this effect revealed that lack of external calcium reduced LactC2-positive PM area by ~50%. Further chelation of cytosolic calcium by BAPTA-AM did not have a notable effect, suggesting that extracellular calcium is a major mediator of this effect (Fig. 4C).

Finally, we hypothesized that since activation-induced PM scrambling was occurring in healthy cells undergoing physiological signaling, it would be reversed after the activating stimulus was resolved. To test reversibility, we imaged PS exposure in RBL cells by staining with LactC2 at various time points after inducing activation. We observed that PS puncta peaked within 15 min after activation and plateaued at that level for ~1.5 h before reversing back to steady-state levels by ~4 h (*i.e.* almost no detectable staining, Fig. 4D).

Discussion

The release of steady-state lipid asymmetry, *i.e.* lipid scrambling, has been implicated in several physiological contexts, most notably apoptosis[15–17] and blood clotting,[20,23] but also cell–cell fusion[24–28] and immune signaling.[31–34] Here, we report that activation of immune cells produces reversible, calcium-dependent scrambling of the PM, distinguished by local foci of surface-exposed PS, PE, and possibly other inner leaflet phospholipids (Fig. 1 and 2). Observations of low lipid packing in these foci (Fig. 3) are consistent with these findings, as inner leaflet lipid classes like PS and PE are typically more unsaturated than outer leaflet

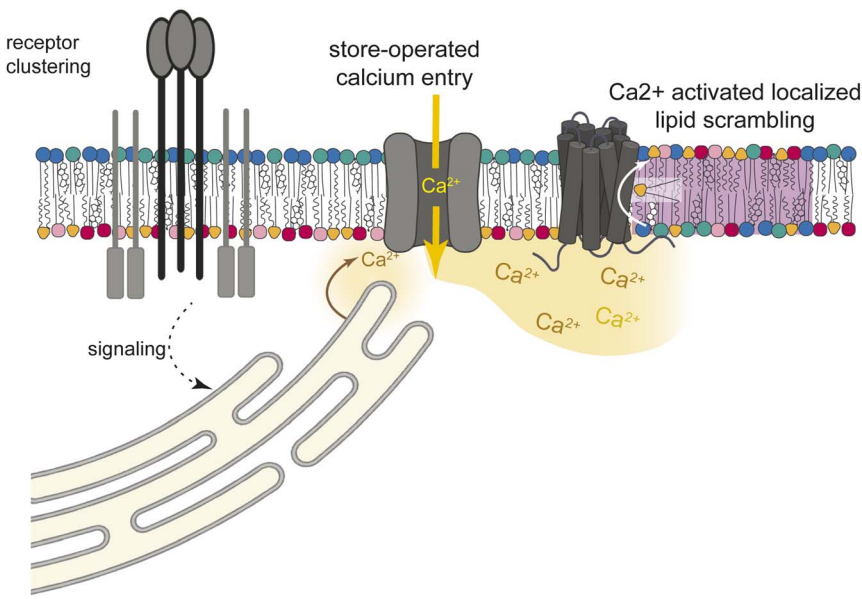

Fig. 5 Schematic of hypothesized cellular mechanism of lipid scrambling downstream of immune activation. Engagement of immune receptors activates calcium mobilization through IP3 and SOCE. The resulting increase in intracellular calcium activates PM resident scramblases to locally release lipid asymmetry.

lipids,[2,49,50] thus their scrambling would introduce unsaturated lipids into the typically tightly packed outer leaflet.[2]

The calcium-dependence of the scrambled foci (Fig. 4A and B) leads us to speculate that they are mediated by calcium-induced activation of members of the scramblase TMEM16 family[18] by calcium mobilized during immune activation. Namely, engagement of antigen receptors leads to phosphorylation and consequent activation of phospholipase C, resulting in production of inositol-1,4,5-trisphosphate (IP3). IP3 in turn activates the ER-resident IP3 Receptor (IP3R) to trigger release of Ca^{2+} from ER stores (Fig. 5). This ER Ca^{2+} release often triggers further store-operated Ca^{2+} entry (SOCE) through PM channels, an often-necessary Ca^{2+} influx pathway in immune cells in response to antigen receptor engagement.[48] As extracellular Ca^{2+} is required for formation of scrambled foci, SOCE is its likely mechanism.

Unlike lipid scrambling associated with cell death (*e.g.* apoptosis), the scrambled foci we report are reversible (Fig. 4D). However, the foci are long-lived, persisting notably longer than either receptor proximal signaling (*i.e.* phosphorylation of LAT) and even the more distal signaling of ERK phosphorylation (*e.g.* Fig. 1C). How this scrambling is resolved is unclear. Non-exclusive possibilities include flippase-mediated rectification of asymmetry and/or shedding or endocytosis of scrambled membrane regions. Another mystery is why the scrambled lipids persist as foci for >1 h, contrary to the expectation that fast lipid diffusion would quickly eliminate local heterogeneity. It is possible that fast scrambling rates locally outcompete diffusion and enzyme-mediated flipping, producing local structure. A non-exclusive alternative is that scrambled regions are somehow isolated from the rest of the PM.

Most importantly, the cellular consequences of this local scrambling are yet unknown. We speculate that the major changes in local membrane properties (lipid packing, charge, perhaps protein composition) in these foci regulate signaling at the PM. These mechanisms remain to be resolved in future work.

Materials and methods

Cell lines and culture conditions

RBL-2H3 and Jurkat were purchased from ATCC. RBL-2H3 were cultured in EMEM medium supplemented with 10% FBS (Genesee) and 100 U mL^{-1} penicillin and 100 μg mL^{-1} streptomycin (Gibco), while Jurkat cells were cultured in RPMI medium supplemented with 10% FBS (Genesee) and 100 U mL^{-1} penicillin and 100 μg mL^{-1} streptomycin (Gibco). Cells were routinely checked for mycoplasma using an ATCC mycoplasma detection kit. Activation and ionophore treatments were performed with reagents diluted in Tyrode's buffer (135 mM NaCl, 5 mM KCl, 1.8 mM $CaCl_2$, 1 mM $MgCl_2$, 5.6 mM glucose, 20 mM HEPES) (pH 7.4) or Ca^{2+}-free Tyrode's buffer.

Fluorescence lifetime imaging (FLIM) and other microscopy

Cells were incubated with 1 μg mL^{-1} Di-4-ANEPPDHQ (Di4, ThermoFisher D36802) at 4 °C for 10 min in Tyrode's buffer. Cells were briefly washed twice in the same buffer at ambient temperature before imaging at room temperature using a Leica SP8 confocal microscope with white light laser and TCSPC

capabilities with Falcon software. We acquired images using 63× water-immersion objective with 485 nm excitation and emission of 550–800 nm. To prevent any contaminating signal from internalization of the dye, all images were acquired within 20 minutes of staining. The data was fit to two lifetimes with an exponential reconvolution fit and we report the calculated mean intensity-weighted lifetime. For LactC2 imaging, recombinant LactC2-mCherry was added and images were collected with 587 nm excitation and 760 nm emission. All confocal imaging was performed using Leica SP8 confocal microscope using 63× water immersion objective. Total internal reflection fluorescence (TIRF) microscopy was performed using Leica DMi8 Thunder Imager and 63× oil-immersion objective.

Apoptosis and ionophore-treatment scrambling induction

Apoptosis was induced by incubating cells in full medium with 1 μM staurosporine (STS) (S6942, Sigma-Aldrich) for 4 hours at 37 °C. Calcium ionophores A23187 (Cayman Chemical Company, 11016) and ionomycin (Thermo Scientific, J60628) were used to elevate intracellular [Ca^{2+}] and induce PM scrambling – both were freshly dissolved in DMSO and used with a final concentration of 3 μM in Tyrode's buffer for 15 minutes at 37 °C.

Immune cell activation by receptor crosslinking

To induce RBL-2H3 activation, cells were first primed with 1 μg mL^{-1} monoclonal anti-dinitrophenyl mouse IgE (D8406, Sigma-Aldrich) in full medium. Then cells were activated by treating with 1 μg per mL 2,4-dinitrophenylated bovine serum albumin (DNP-BSA) (Invitrogen, A23018) dissolved in PBS as a crosslinking antigen. Activation was performed in Tyrode's buffer or Ca^{2+}-free Tyrode's buffer (Fig. 3A and B). To label the plasma membrane, the IgE was labeled with AlexaFluor-555 using the Alexa Fluor 555 Antibody Labeling Kit (A20187, Thermo Scientific), with the degree of labeling determined to be 3.9 labels per antibody. Jurkat T cells were activated by plating onto a glass coverslip surface coated with monoclonal anti-human CD3 antibody (OKT-3, 317301, BioLegend). Coverslip glass surface was incubated with 5 μg mL^{-1} of OKT-3 in PBS for 30 minutes at 37 °C prior to imaging.[43]

Calcium-chelation/quenching

BAPTA-AM (B6769 Thermo Scientific) was used to chelate intracellular Ca^{2+}. BAPTA-AM was freshly dissolved in DMSO and used at final concentration of 10 μM in Ca^{2+}-free Tyrode's buffer. Cells were pre-treated with BAPTA-AM for 5 minutes before activation and chelator was also present during DNP-BSA antigen activation of RBL-2H3 cells.

Lipid-specific probes

PS-specific probe Annexin V conjugated with Alexa Fluor 647 (AnxV-647) was purchased from Thermo Scientific (A13204). LactadherinC2-mClover construct was expressed and purified in-house, using Co-NTA agarose purification resin (31405, Cube Biotech) and reconstituted in 20 mM HEPES and 150 mM NaCl, pH 7.4 buffer. The expression plasmid was a gift from S. Grinstein (Hospital for Sick

Children, Toronto, Canada). The PE-specific probe duramycin-PEG-GFP[51] was incubated for 30 minutes with RBL cells during DNP-BSA-mediated FceRI activation at final concentration of 10 μg mL^{-1} in Tyrode's buffer. Purified recombinant probe was a generous gift from Ming Zhao (University of Wisconsin–Madison).

Western blot

All primary antibodies were used in 1 : 1000, all secondary – 1 : 10 000, diluted in 5% BSA in TBS-T blocking buffer. Primary antibodies: anti-ERK1/ERK2 (E.657.8) (Invitrogen, MA5-15227), anti-phospho-ERK1/ERK2 (Tyr204) (B.742.5) (Invitrogen, MA-15174), anti-LAT (phospho Y200) antibody [EP983(2)Y] (Abcam, ab68139), anti-LAT (E3U6J) (Cell Signaling, 45533S), anti-Calnexin (Abcam, ab22595). Secondary antibodies: anti-rabbit IgG, HRP linked antibody (Cell Signaling, 7074S), anti-mouse IgG, HRP-linked antibody (Cell Signaling, 7076).

Flow cytometry

RBL cells were first primed with 1 μg mL^{-1} monoclonal anti-dinitrophenyl mouse IgE (D8406, Sigma-Aldrich) in full medium at 37 °C for 1 h. Then cells were activated by treating with 1 μg mL^{-1} DNP-BSA in Tyrode's buffer for 15 min at 37 °C. A parallel set of cells was incubated with ionomycin in Tyrode's buffer for 15 min at 37 °C. AnxV-488 was added to the cells for 5 min before performing flow cytometry on an LSR Fortessa. Viable cells were gated on forward- and side-scatter, and the AnxV intensity was plotted as a histogram of viable cells.

Data availability

All data relevant to this publication are included in the figures. Primary datasets including imaging data and raw Western blots are freely publicly available *via* UVA Dataverse (**https://doi.org/10.18130/V3/RTP9A2**), a public institutional repository that is part of the Libra Scholarly Repository.

Conflicts of interest

There are no conflicts to declare.

Acknowledgements

TIRF microscopy was performed at the Advanced Microscopy Facility at the University of Virginia. Funding for this work was provided by the NIH (GM134949, AI183581, F32GM134704, F31AI181453) and the Owens Foundation.

References

1 P. F. Devaux, Static and dynamic lipid asymmetry in cell membranes, *Biochemistry*, 1991, **30**(5), 1163–1173.
2 J. H. Lorent, *et al.*, Plasma membranes are asymmetric in lipid unsaturation, packing and protein shape, *Nat. Chem. Biol.*, 2020, **16**(6), 644–652.

3 Y. Zhou, *et al.*, Membrane potential modulates plasma membrane phospholipid dynamics and K-Ras signaling, *Science*, 2015, **349**(6250), 873–876.
4 T. Banerjee, *et al.*, Spatiotemporal dynamics of membrane surface charge regulates cell polarity and migration, *Nat. Cell Biol.*, 2022, **24**(10), 1499–1515.
5 H. M. Hankins, *et al.*, Role of flippases, scramblases and transfer proteins in phosphatidylserine subcellular distribution, *Traffic*, 2015, **16**(1), 35–47.
6 A. Gupta, *et al.*, Plasma membrane asymmetry of lipid organization: fluorescence lifetime microscopy and correlation spectroscopy analysis, *J. Lipid Res.*, 2020, **61**(2), 252–266.
7 Y. Elani, *et al.*, Measurements of the effect of membrane asymmetry on the mechanical properties of lipid bilayers, *Chem. Commun.*, 2015, **51**(32), 6976–6979.
8 A. Hossein and M. Deserno, Stiffening transition in asymmetric lipid bilayers: The role of highly ordered domains and the effect of temperature and size, *J. Chem. Phys.*, 2021, **154**(1), 014704.
9 S. L. Foley, *et al.*, Elastic and thermodynamic consequences of lipid membrane asymmetry, *Emerging Top. Life Sci.*, 2023, **7**(1), 95–110.
10 S. Shukla and T. Baumgart, Enzymatic trans-bilayer lipid transport: Mechanisms, efficiencies, slippage, and membrane curvature, *Biochim. Biophys. Acta, Biomembr.*, 2021, **1863**(3), 183534.
11 K. Balasubramanian and A. J. Schroit, Aminophospholipid asymmetry: A matter of life and death, *Annu. Rev. Physiol.*, 2003, **65**, 701–734.
12 K. M. Kodigepalli, *et al.*, Roles and regulation of phospholipid scramblases, *FEBS Lett.*, 2015, **589**(1), 3–14.
13 T. Yeung, *et al.*, Membrane phosphatidylserine regulates surface charge and protein localization, *Science*, 2008, **319**(5860), 210–213.
14 T. Yeung, *et al.*, Receptor activation alters inner surface potential during phagocytosis, *Science*, 2006, **313**(5785), 347–351.
15 K. Segawa, *et al.*, Caspase-mediated cleavage of phospholipid flippase for apoptotic phosphatidylserine exposure, *Science*, 2014, **344**(6188), 1164–1168.
16 J. Suzuki, *et al.*, Xk-related protein 8 and CED-8 promote phosphatidylserine exposure in apoptotic cells, *Science*, 2013, **341**(6144), 403–406.
17 U. Sivagnanam, S. K. Palanirajan and S. N. Gummadi, The role of human phospholipid scramblases in apoptosis: An overview, *Biochim. Biophys. Acta*, 2017, **1864**(12), 2261–2271.
18 T. Sakuragi and S. Nagata, Regulation of phospholipid distribution in the lipid bilayer by flippases and scramblases, *Nat. Rev. Mol. Cell Biol.*, 2023, **24**, 576–596.
19 J. Suzuki, *et al.*, Calcium-dependent phospholipid scramblase activity of TMEM16 protein family members, *J. Biol. Chem.*, 2013, **288**(19), 13305–13316.
20 J. Suzuki, *et al.*, Calcium-dependent phospholipid scrambling by TMEM16F, *Nature*, 2010, **468**(7325), 834–838.
21 M. Doktorova, *et al.*, Cell membranes sustain phospholipid imbalance via cholesterol asymmetry, *Cell*, 2025, DOI: **10.1016/j.cell.2025.02.034**.
22 J. Ousingsawat, *et al.*, Contribution of TMEM16F to pyroptotic cell death, *Cell Death Dis.*, 2018, **9**(3), 300.

23 R. F. Zwaal, P. Comfurius and E. M. Bevers, Surface exposure of phosphatidylserine in pathological cells, *Cell. Mol. Life Sci.*, 2005, **62**(9), 971–988.
24 Y. Zhang, *et al.*, TMEM16F phospholipid scramblase mediates trophoblast fusion and placental development, *Sci. Adv.*, 2020, **6**(19), eaba0310.
25 J. M. Whitlock, *et al.*, Anoctamin 5/TMEM16E facilitates muscle precursor cell fusion, *J. Gen. Physiol.*, 2018, **150**(11), 1498–1509.
26 S. K. Verma, *et al.*, Cell-surface phosphatidylserine regulates osteoclast precursor fusion, *J. Biol. Chem.*, 2018, **293**(1), 254–270.
27 C. M. Rival, *et al.*, Phosphatidylserine on viable sperm and phagocytic machinery in oocytes regulate mammalian fertilization, *Nat. Commun.*, 2019, **10**(1), 4456.
28 M. Tsuchiya, *et al.*, Cell surface flip-flop of phosphatidylserine is critical for PIEZO1-mediated myotube formation, *Nat. Commun.*, 2018, **9**(1), 2049.
29 E. Cocucci and J. Meldolesi, Ectosomes and exosomes: shedding the confusion between extracellular vesicles, *Trends Cell Biol.*, 2015, **25**(6), 364–372.
30 J. M. Whitlock and H. C. Hartzell, Anoctamins/TMEM16 Proteins: Chloride Channels Flirting with Lipids and Extracellular Vesicles, *Annu. Rev. Physiol.*, 2017, **79**, 119–143.
31 K. Fischer, *et al.*, Antigen recognition induces phosphatidylserine exposure on the cell surface of human $CD8^+$ T cells, *Blood*, 2006, **108**(13), 4094–4101.
32 S. R. Dillon, *et al.*, Annexin V binds to viable B cells and colocalizes with a marker of lipid rafts upon B cell receptor activation, *J. Immunol.*, 2000, **164**(3), 1322–1332.
33 S. C. Frasch, *et al.*, Phospholipid flip-flop and phospholipid scramblase 1 (PLSCR1) co-localize to uropod rafts in formylated Met-Leu-Phe-stimulated neutrophils, *J. Biol. Chem.*, 2004, **279**(17), 17625–17633.
34 S. Martin, *et al.*, Immunologic stimulation of mast cells leads to the reversible exposure of phosphatidylserine in the absence of apoptosis, *Int. Arch. Allergy Immunol.*, 2000, **123**(3), 249–258.
35 N. Wu, *et al.*, Critical Role of Lipid Scramblase TMEM16F in Phosphatidylserine Exposure and Repair of Plasma Membrane after Pore Formation, *Cell Rep.*, 2020, **30**(4), 1129.
36 K. Emoto and M. Umeda, An essential role for a membrane lipid in cytokinesis. Regulation of contractile ring disassembly by redistribution of phosphatidylethanolamine, *J. Cell Biol.*, 2000, **149**(6), 1215–1224.
37 A. MacKenzie, *et al.*, Rapid secretion of interleukin-1β by microvesicle shedding, *Immunity*, 2001, **15**(5), 825–835.
38 N. Wu, H. Song and A. Veillette, Plasma membrane lipid scrambling causing phosphatidylserine exposure negatively regulates NK cell activation, *Cell. Mol. Immunol.*, 2021, **18**(3), 686–697.
39 A. Connolly, *et al.*, TMEM16F mediates bystander TCR-CD3 membrane dissociation at the immunological synapse and potentiates T cell activation, *Sci. Signaling*, 2021, **14**(675), eabb5146.
40 Y. Hu, *et al.*, Scramblase TMEM16F terminates T cell receptor signaling to restrict T cell exhaustion, *J. Exp. Med.*, 2016, **213**(12), 2759–2772.
41 A. M. Gilfillan and C. Tkaczyk, Integrated signalling pathways for mast-cell activation, *Nat. Rev. Immunol.*, 2006, **6**(3), 218–230.

42 M. Vig and J. P. Kinet, Calcium signaling in immune cells, *Nat. Immunol.*, 2009, **10**(1), 21–27.
43 H. Y. Wang, *et al.*, Coupling of protein condensates to ordered lipid domains determines functional membrane organization, *Sci. Adv.*, 2023, **9**(17), eadf6205.
44 R. Kreder, *et al.*, Solvatochromic Nile Red probes with FRET quencher reveal lipid order heterogeneity in living and apoptotic cells, *ACS Chem. Biol.*, 2015, **10**(6), 1435–1442.
45 Z. Darwich, *et al.*, Detection of apoptosis through the lipid order of the outer plasma membrane leaflet, *Biochim. Biophys. Acta*, 2012, **1818**(12), 3048–3054.
46 D. M. Owen, *et al.*, Quantitative imaging of membrane lipid order in cells and organisms, *Nat. Protoc.*, 2012, **7**(1), 24–35.
47 D. M. Owen, *et al.*, Fluorescence lifetime imaging provides enhanced contrast when imaging the phase-sensitive dye di-4-ANEPPDHQ in model membranes and live cells, *Biophys. J.*, 2006, **90**(11), L80–L82.
48 S. Feske, Immunodeficiency due to defects in store-operated calcium entry, *Ann. N. Y. Acad. Sci.*, 2011, **1238**, 74–90.
49 K. R. Levental, *et al.*, ω-3 polyunsaturated fatty acids direct differentiation of the membrane phenotype in mesenchymal stem cells to potentiate osteogenesis, *Sci. Adv.*, 2017, **3**(11), eaao1193.
50 K. R. Levental, *et al.*, Lipidomic and biophysical homeostasis of mammalian membranes counteracts dietary lipid perturbations to maintain cellular fitness, *Nat. Commun.*, 2020, **11**(1), 1339.
51 S. Hou, S. E. Johnson and M. Zhao, A One-Step Staining Probe for Phosphatidylethanolamine, *ChemBioChem*, 2015, **16**(13), 1955–1960.